

# Quasi-Orthogonal Wideband Radar Waveforms Based on Chaotic Systems\*

Matt S. Willsey<sup>+</sup>, Kevin M. Cuomo<sup>†</sup>, *Member, IEEE*, and Alan V. Oppenheim<sup>‡</sup>, *Life Fellow, IEEE*

## Abstract

Many radar applications, such as those involving multiple-input, multiple-output (MIMO) radar, require sets of waveforms that are orthogonal, or nearly orthogonal. As shown in this paper, a set of nearly orthogonal waveforms with a high cardinality can be generated using chaotic systems, and this set performs comparably to other waveform sets used in pulse compression radar systems. Specifically, the nearly orthogonal waveforms from chaotic systems are shown to possess many desirable radar properties including a compact spectrum, low range sidelobes, and an average transmit power within a few dB of peak power. Moreover, these waveforms can be generated at essentially any practical time length and bandwidth. Since these waveforms are generated from a deterministic process, each waveform can be represented with a small number of system parameters. Additionally, assuming these waveforms possess a large time-bandwidth product, a high number of nearly-orthogonal chaotic waveforms exist for a given time and bandwidth. Thus, the proposed generation procedure can potentially be used to generate a new transmit waveform on each pulse.

## Index Terms

Radar, Waveforms, Chaos, Lorenz, MIMO Radar, Quasi-Orthogonal, Waveform Set.

## I. INTRODUCTION

The study of waveform design for pulse compression radar systems has given rise to a wide variety of classes of waveforms aimed at satisfying specified design constraints. Typically, these systems utilize a matched filter to achieve high range resolution and to maximize the signal-to-noise ratio (SNR) in Gaussian noise [1]. As a result of utilizing the matched filter, transmit waveforms with low autocorrelation function sidelobes are desired to prevent false alarms and prevent stronger returns from masking the presence of weaker returns. Several sets of waveforms, such as those utilizing Barker codes [2] and maximal length sequences [3], achieve low autocorrelation function sidelobes. Unfortunately, drawbacks to these waveforms can include spectral leakage, peak power limitations, and the

\* This work is sponsored in part under Air Force Contract FA8721-05-C-0002. Opinions, interpretations, recommendations and conclusions are those of the authors and are not necessarily endorsed by the United States Government.

<sup>+</sup> Matt S. Willsey was with the Research Laboratory of Electronics while the research for this manuscript was conducted.

<sup>†</sup> Kevin M. Cuomo (cuomo@ll.mit.edu) is with M.I.T. Lincoln Laboratory.

<sup>‡</sup> Alan V. Oppenheim (avo@mit.edu) is with Research Laboratory of Electronics and is supported in part by Lincoln Laboratory PO 7000032361 and by the Texas Instruments Leadership University Program.

computational complexity of receive processing. On the other hand, linear frequency modulated (LFM) waveforms possess acceptable autocorrelation function sidelobe levels while satisfying practical considerations such as reduced spectral leakage, average power levels within a few dB of peak power, and computationally inexpensive receiver implementations ([5] and [2]). Additionally, LFM waveforms are robust to Doppler errors<sup>1</sup> - as illustrated by examining Woodward's ambiguity function [4]. These properties have made the LFM the waveform of choice for many practical radar applications.

In some applications, however, the use of orthogonal transmit waveforms is required. For example, in multiple-input, multiple-output (MIMO) radar systems, using multiple transmit and receive elements provides increased sensitivity, desired transmit beam patterns, and allows advanced surveillance techniques ([6], [7], [8], and [9]). In some modes of operation for MIMO systems, a large set of orthogonal waveforms is desired to prevent cross-talk between elements operating simultaneously in the same band. An orthogonal waveform set implies that the cross-ambiguity surface equals zero for all combinations of waveforms in the set. However, as presented in [10], the height of the cross-ambiguity surface of any two waveforms (and more generally the MIMO radar ambiguity surface of  $K$  waveforms) cannot everywhere equal zero. Fortunately, sets of waveforms possessing cross-ambiguity functions with a maximum height that is small relative to the peak of the ambiguity surfaces are acceptable in many applications and will be referred to as quasi-orthogonal. Assuming the peak of each ambiguity surface is roughly equal for two quasi-orthogonal waveforms, the level of the normalized cross-ambiguity surface (normalized by the ambiguity surface peak) is at a level roughly equal to  $-10 \log(TB)$  dB where  $TB$  corresponds to the time-bandwidth product<sup>2</sup>.

There are many existing techniques capable of generating quasi-orthogonal waveform sets. A set of Gaussian noise waveforms, as discussed in [11] or [12] for example, has a high number of distinct quasi-orthogonal waveforms. However, such waveforms often result in a loss in signal-to-noise ratio when compared to waveforms that have a nearly constant transmit envelope. In [13], waveforms based on hyperbolic frequency hopped codes of length  $N$  can achieve a low cross-correlation function baseline while maintaining an average transmit power level that is within a few dB of peak power. These waveforms are limited by a cardinality less than  $N$ , and only exist when  $N$  is a prime integer. Additionally, waveforms based on frequency/phase modulation of a discontinuous codes often lead to spectral leakage.

In this paper we develop a new waveform design technique that exploits the chaotic behavior of non-linear dynamical systems to generate a quasi-orthogonal set with a high cardinality. The use of deterministic chaos in waveform design has been proposed previously. Some techniques, for example, use continuous-time solutions of chaotic systems as radar waveforms (such as in [14]). The resulting waveforms possess properties similar to waveforms based on Gaussian noise that might include an SNR loss when compared to waveforms with a constant

<sup>1</sup>Although the LFM waveforms are robust to Doppler errors, a Doppler error will introduce a corresponding error in range.

<sup>2</sup>To simplify the discussion from this point forward, the cross-correlation function, a zero-Doppler slice of the cross-ambiguity function, will be used to characterize the quasi-orthogonality of two waveforms and must also have a normalized level roughly equal to  $-10 \log(TB)$  dB.

envelope. Other design techniques use chaotic maps in phase/frequency modulation (such as in [15]), which, as mentioned in the previous paragraph, could limit the cardinality and lead to spectral leakage.

Our approach to providing a quasi-orthogonal waveform set is a two-step process that first generates signals from chaotic systems and then modifies these signals based on our desired radar waveform performance considerations (presented in the following sections). These waveforms are empirically shown to have cross-correlation and autocorrelation function sidelobes at a level roughly equal to  $-10 \log(TB)$  dB, arbitrary time lengths and bandwidths, and can be constructed in a way that reduces spectral leakage while maintaining an average transmit power within a few dB of peak power. Because these waveforms are generated by a deterministic system, specified by a small number of system parameters, they can be efficiently generated in the transmitter and receiver<sup>3</sup>. Consequently, they are well-suited for real-time orthogonal waveform generation and processing. These attributes of chaotic waveforms make them an interesting class of waveforms to consider for a variety MIMO radar applications requiring ease of generation, compact frequency spectrum, efficient power levels, and space-time orthogonality.

## II. RADAR WAVEFORM DESIGN CONSIDERATIONS

This section presents the criteria by which radar waveforms are evaluated. A typical transmit radar waveform  $s(t)$  is an amplitude and phase modulated sinusoid of the form in Eq. 1 where  $a(t)$  and  $\theta(t)$  are slowly varying relative to the center frequency  $\omega_c$  [2]. Such signals will have spectral energy concentrated around  $\pm\omega_c$  [2]. However, for simplicity, the waveforms discussed in this paper will be used as the complex envelope of  $s(t)$ . The complex envelope,  $\mu(t)$ , is related to  $s(t)$  via Eq. 2.

$$s(t) = a(t) \cos(\omega_c t + \theta(t)) \quad (1)$$

$$s(t) = \Re\{\mu(t)e^{j\omega_c t}\} \quad (2)$$

Various constraints and performance metrics have been grouped into four design considerations used in evaluating  $\mu(t)$  [16]. These considerations are briefly discussed below.

### A. Average Transmit Power

Practical radar systems often have power limitations that require constant envelope transmit waveforms so that the average transmit power is within a few dB of peak power. The peak-to-RMS ratio (PRMS) of the transmit signal  $s(t)$  quantifies this loss in transmit power, and low PRMS values are desired. The PRMS of the transmit waveform  $s(t)$  is related to the PRMS of the complex envelope  $\mu(t)$  via Eq. 3.

$$s_{prms} = \sqrt{2}\mu_{prms} \quad (3)$$

<sup>3</sup>Efficient generation of these waveforms is discussed further in Section VI.

### B. Range Resolution and Sidelobes

For practical pulse compression systems utilizing the matched filter, the autocorrelation function, as defined in Eq. 4, is an important design consideration<sup>4</sup>.

$$r_{\mu\mu}(t) = \int_{-\infty}^{\infty} \mu(\tau) \mu^*(\tau - t) d\tau \quad (4)$$

Specifically, a narrow mainlobe is required to resolve targets closely spaced in range, and low sidelobes are necessary to prevent larger targets from interfering with smaller targets or creating false alarms. For illustrative purposes, we will show plots of the autocorrelation function normalized by  $\int_{-\infty}^{\infty} |\mu(\tau)|^2 d\tau$  so that the peak is unity.

### C. Spectral Leakage

Spectral leakage refers to radiating significant energy outside the specified transmit band of a system, which will be referred to as out-of-band energy. Out-of-band energy can interfere with other radar and communication systems and be intercepted by an adversary. Additionally, if the transmit waveform possesses too much out-of-band energy, the sensitivity of the radar can be reduced, since this energy is often attenuated by the transmitter. Based on the specifications and constraints of this application, the out-of-band energy needs to be appropriately limited. The energy density spectrum is used to quantify the amount of out-of-band energy and is calculated according to Eq. 5 where  $M(f)$  is the Fourier transform of  $\mu(t)$  and  $f$  and  $t$  are in units of Hz and s, respectively.

$$\Phi_{\mu\mu}(f) = M(f)M^*(f) \quad (5)$$

The energy density spectrum will be referred to as the energy spectrum from this point forward. For illustrative purposes, the energy spectrum will be normalized in plots so that the average energy in the transmit band is equal to 0 dB.

### D. Orthogonality

As discussed in the Section I, some applications require a quasi-orthogonal waveform set with a high cardinality. Since pulse compression systems utilize the matched filter, the cross-correlation, as defined in Eq. 6, measures the interference of one waveform when processing a second waveform belonging to the set.

$$r_{\mu\nu}(t) = \int_{-\infty}^{\infty} \mu(\tau) \nu^*(\tau - t) d\tau \quad (6)$$

For illustrative purposes, the cross-correlation function, like the autocorrelation function, is normalized by  $\int_{-\infty}^{\infty} |\mu(t)|^2 dt$ , which is approximately equal to  $\int_{-\infty}^{\infty} |\nu(t)|^2 dt$  for the waveforms discussed herein. Two waveforms (of equal length  $T$  and bandwidth  $B$ ) are considered quasi-orthogonal if the normalized cross-correlation function is roughly equal to  $-10 \log(TB)$  dB.

<sup>4</sup>To simplify this discussion, the Doppler effect has been ignored.

### III. GENERATING RADAR WAVEFORMS WITH CHAOTIC SYSTEMS

As similarly presented in [17], solutions to chaotic equations are bounded, aperiodic, and possess a sensitivity to initial conditions. Unlimited numbers of continuous-time chaotic systems do exist [18], and there are several well-known, continuous-time chaotic systems such as the Lorenz system, the Rössler system, and the Double Scroll system. This paper describes the use of, perhaps, the most well-known chaotic system, the Lorenz system. Many of the concepts and tools developed herein can also be extended to these other chaotic systems.

#### A. The Lorenz System

The Lorenz system is a well-studied chaotic system [19] and is given in Eq. 7.

$$\begin{aligned}\dot{x} &= \sigma(y - x) \\ \dot{y} &= rx - y - xz \\ \dot{z} &= xy - bz\end{aligned}\tag{7}$$

The three parameters  $\sigma$ ,  $r$ , and  $b$  are referred to as the Lorenz parameters. The Lorenz parameters must satisfy the constraints in Eqs. 8 - 10 so that the Lorenz system gives rise to chaotic dynamics.

$$b > 0\tag{8}$$

$$\sigma > b + 1\tag{9}$$

$$r > \frac{\sigma(\sigma + b + 3)}{(\sigma - b - 1)} \equiv r_c.\tag{10}$$

The variable  $r_c$  in Eq. 10 is used to denote the critical value of  $r$ . All chaotic solutions to the Lorenz Eqs. will converge to a set called an attractor.

Many advantages of using chaotic systems to generate radar waveforms can be intuitively understood from the properties of chaotic trajectories: boundedness, aperiodicity, and sensitivity to initial conditions. For example, the bounded nature of trajectories leads to a low PRMS. The aperiodic flow leads to low autocorrelation and cross-correlation sidelobes, and the sensitivity to initial conditions gives rise to the quasi-orthogonality of chaotic waveforms.

#### B. Generating Lorenz Waveforms

Waveforms generated from the Lorenz equations will be referred to as Lorenz waveforms and will be derived from the state variables of the Lorenz equations, which are approximated by numerically integrating Eq. 7 using a fourth-order Runge-Kutta method with  $10^{-3}$  seconds for the step size<sup>5</sup>. Preliminary empirical studies showed the state variable  $x(t)$  possessed better waveform properties than  $y(t)$  or  $z(t)$ . Moreover, no empirical evidence

<sup>5</sup>As will be discussed in Section IV, a simplification will be used to map the Runge-Kutta step size of  $10^{-3}$  to a smaller sampling period to allow larger bandwidths.

suggested that a linear combination of state variables would yield significant improvement over  $x(t)$ . Thus as a simplification, all radar waveforms are obtained from  $x(t)$ .

A Lorenz waveform,  $x_L(t)$ , will be defined as a normalized, time-windowed segment of the  $x$ -state-variable as shown in Eq. 11 where  $T$  denotes the length of the waveform in time and  $x_p$  denotes the maximum of  $|W_r(t)x(t + \tau_a)|$ .

$$x_L(t) = \frac{1}{x_p} W_r(t) x(t + \tau_a) \quad (11)$$

$$W_r(t) = \begin{cases} 1; & t \in [0, T] \\ 0; & \text{else} \end{cases} \quad (12)$$

The state variable  $x(t)$  is advanced by  $\tau_a$  so that the solutions of Eq. 7, with randomly-selected initial conditions at  $t = 0$ , have enough time to converge to the attractor before the Lorenz waveform is extracted. This convergence time can be limited by randomly selecting points nearby the attractor as initial conditions. Additionally, when generating  $x(t)$  from Eq. 7, the Lorenz parameters are selected according to Eq. 13, where  $r_c$  is given in Eq. 10. This parameter selection is empirically shown in [16] to minimize the autocorrelation function sidelobes and give rise to a PRMS ratio less than 2.3.

$$\{\sigma, r, b\} = a\{267, r_c + 0.01, 100\} \quad (13)$$

The bandwidth can be adjusted by scaling the parameters by  $a$ , which approximately corresponds to scaling the bandwidth of  $x_L(t)$  by  $a$  when  $a \in [0.4, \infty)$  and  $r > 360$  [16].

#### IV. COMPARISON OF THE LORENZ WAVEFORMS WITH TRADITIONAL DESIGNS

In this section, the Lorenz waveforms are generated to meet the specifications in Table I and are evaluated using the metrics and considerations described in Section II. For reference, the performance of the Lorenz waveform set will be compared with a set of quasi-orthogonal waveforms generated from pseudo-random sequences that also satisfy the system specifications in Table I. The performance of a sample waveform from each set will be compared to illustrate typical results. The variables  $x_L(t)$  and  $w(t)$  correspond to a Lorenz and a pseudo-random noise waveform, respectively.

Before the Lorenz waveforms can be generated, the Lorenz parameters in Eq. 13 need to be selected to meet the specifications in Table I. Before determining the value of these parameters, a simplification is introduced to prevent extremely large values from being selected as Lorenz parameters. As explained previously, the Lorenz equations in Eq. 7 are numerically integrated with a step size of  $10^{-3}$  to give a discrete-time signal. By assuming the unit time of the Lorenz system is  $2/3 \mu\text{s}$  (not 1 s), using a step size of  $10^{-3}$  gives a sampling period of  $2/3$  of a nanosecond, a sampling frequency of 1.5 GHz (in Table I), and reduces the magnitude of the Lorenz parameters needed to achieve the required bandwidth of 500 MHz (in Table I). With this assumption,  $a$  in Eq. 13 is set to 1.65 so that roughly 98% of the content of the energy spectrum of the Lorenz waveform falls within a 500 MHz

Description of System Specifications	
Bandwidth	$B \approx 500 \text{ MHz}$
Pulse Length	$T = 20\mu s$
Sampling Frequency	$f_s = 1.5 \text{ GHz}$

TABLE I  
SYSTEM SPECIFICATIONS.

band centered at  $f = 0$ . The Lorenz equations with these parameters are repeated below in Eq. 14. The parameter values shown in this equation have been rounded to the nearest integer value for notational simplicity.

$$\begin{aligned}
 \dot{x} &= 441 \cdot (y - x) \\
 \dot{y} &= 982 \cdot x - y - xz \\
 \dot{z} &= xy - 165 \cdot z
 \end{aligned} \tag{14}$$

Finally, a Lorenz waveform is extracted according to Eqs. 11 and 12 with  $T$  equal to  $20\mu s$ .

#### A. Average Transmit Power

Using the definition of PRMS from Section II, the average transmit power relative to the peak power can be calculated for both waveforms. The PRMS of the Lorenz waveform,  $x_L(t)$ , is 2.23, which corresponds to a 10 dB loss<sup>6</sup> from peak transmit power. However, the PRMS of  $w(t)$  is 1.21, which corresponds to only a 4.7 dB loss from peak transmit power. Thus, the average transmit power of  $w(t)$  is about 5 dB higher than the average transmit power of  $x_L(t)$ . However, in the Section V, a transformation is presented that modifies the Lorenz waveform to decrease the PRMS.

#### B. Range Resolution and Sidelobes

The range resolution and sidelobes, which correspond to the autocorrelation function mainlobe width and sidelobes, can be compared for  $x_L(t)$  and  $w(t)$ . The autocorrelation function for  $x_L(t)$ ,  $r_{x_L x_L}(t)$ , is given in Fig. 1 and is typical of the autocorrelation function for all Lorenz waveforms. The autocorrelation function of  $w(t)$ ,  $r_{ww}(t)$ , is given in Fig. 2. The average sidelobes for  $r_{x_L x_L}(t)$  are at -43 dB and are slightly higher than the average sidelobes of  $r_{ww}(t)$  at -44 dB. More importantly, the mainlobe of  $r_{x_L x_L}(t)$  is roughly three times wider than  $r_{ww}(t)$ . This increased mainlobe width of the Lorenz waveform is mostly caused by an inefficient utilization of the transmit band as illustrated in the following section.

<sup>6</sup>The loss from peak transmit power,  $L_P$ , is  $L_P = 10 \log(|s_{prms}|^2)$ , which corresponds to  $L_P = 10 \log(2 \cdot |\mu_{prms}|^2)$  according to Eq. 3.

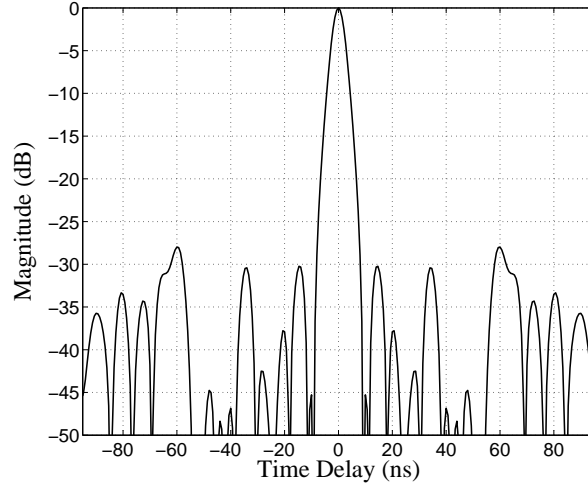


Fig. 1. Normalized Autocorrelation Function of a Lorenz Waveform.

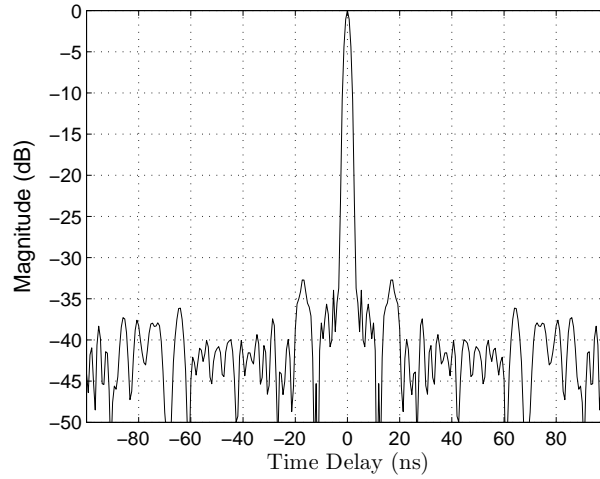


Fig. 2. Normalized Autocorrelation Function for  $w(t)$ .

### C. Spectral Leakage

Preventing spectral leakage requires the concentration of energy spectrum content within the 500 MHz transmit band. The energy spectrum of  $x_L(t)$ ,  $\Phi_{x_L x_L}(f)$ , is given in Fig. 3 and is typical of the spectrum of Lorenz waveforms. The energy spectrum of  $w(t)$ ,  $\Phi_{ww}(f)$ , is given in Fig. 4. While the out-of-band content for each waveform is small,  $\Phi_{ww}(f)$  has a more uniform in-band energy distribution than  $\Phi_{x_L x_L}(f)$ , which leads to an increased waveform bandwidth. Whereas the system bandwidth ( $B$ ) is specified in Table 1, the waveform bandwidth can be calculated using a second moment expression of the spectrum (such as the one in [20]). As explained in [20], the autocorrelation function mainlobe width of  $r_{ww}(t)$  can be narrower than that of  $r_{x_L x_L}(t)$  as a result of this increased bandwidth.



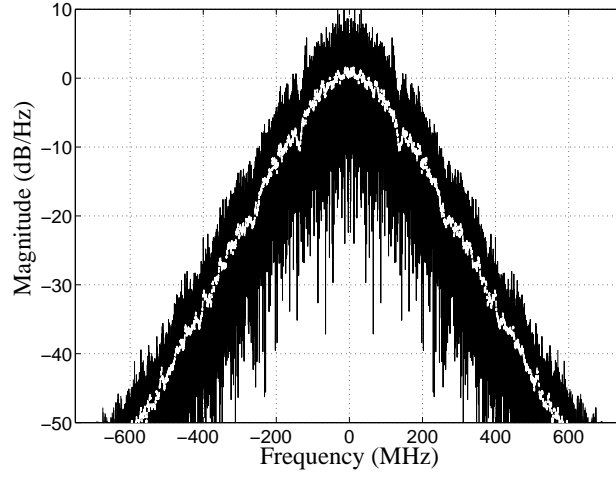


Fig. 3. The Normalized Energy Spectrum of a Lorenz Waveform. The black line is the energy spectrum of a typical transmit waveform and is calculated using Eq. 5. The gray line is used to approximate the average spectrum level for the set of waveforms and is calculated by smoothing the spectrum of a sample transmit waveform.

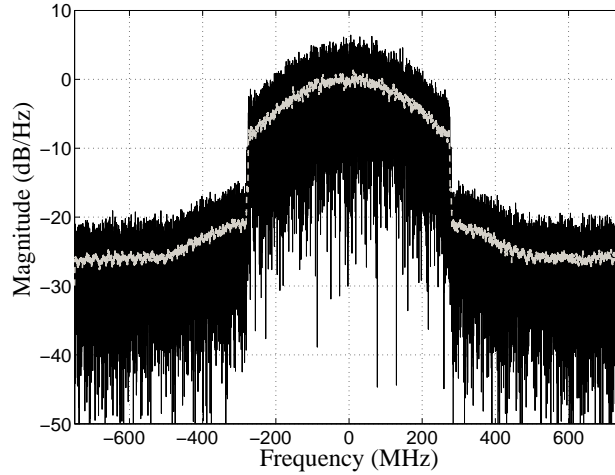


Fig. 4. The Normalized Energy Spectrum of  $w(t)$ . The black line is the energy spectrum of a typical transmit waveform and is calculated using Eq. 5. The gray line is used to approximate the average spectrum level for the set of waveforms and is calculated by smoothing the spectrum of a sample transmit waveform.

#### D. Orthogonality

The normalized cross-correlation level for quasi-orthogonal waveforms is necessarily at a level roughly equal to  $-10 \log(TB)$  dB, which equals  $-40$  dB according to the specifications for  $T$  and  $B$  in Table 1. As illustrated using two sample waveforms from each set (both Lorenz and pseudo-random noise sets), the normalized cross-correlation levels of both sets are indeed roughly equal to  $-40$  dB as shown in Figs. 5 and 6. The cross-correlation level illustrated with these figures is typical of any two waveforms in each respective set.

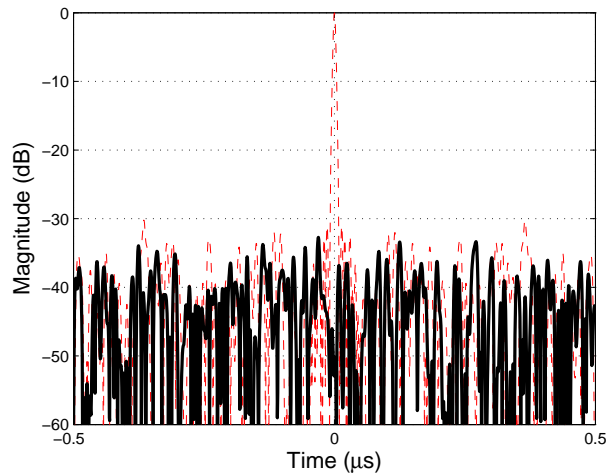


Fig. 5. Normalized Cross-Correlation Function of Two Distinct Lorenz Waveforms. The normalized cross-correlation function (solid line) is roughly equal to  $-10 \log(TB) = -40$  dB. The normalized autocorrelation function is plotted (dashed line) lightly in the background for reference.

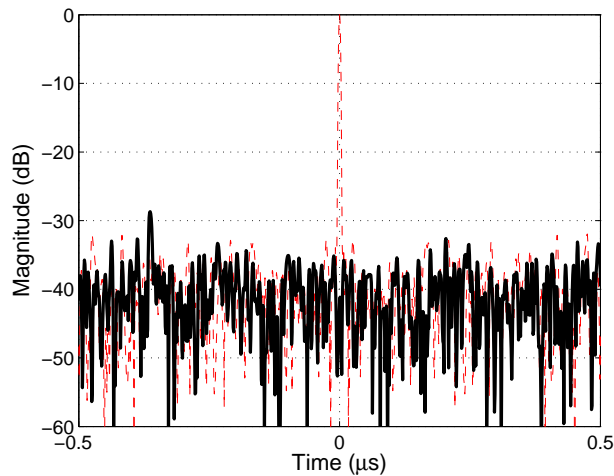


Fig. 6. Normalized Cross-Correlation Function of Pseudo-Random Noise Waveforms. The normalized cross-correlation function (solid line) of two quasi-orthogonal, pseudo-random noise waveforms is on the order of  $-10 \log(TB) = -40$  dB. The normalized autocorrelation function is plotted (dashed line) lightly in the background.

## V. TRANSFORMATIONS TO IMPROVE THE LORENZ RADAR WAVEFORMS

As seen above, Lorenz waveforms possess a lower average power and a decreased waveform bandwidth when compared to the pseudo-random noise waveform that is shown for reference. However, due to a naturally tapered spectrum and bounded dynamics, Lorenz waveforms can be modified to increase the average transmit power and make the spectrum more compact by increasing the bandwidth of the waveform. These modifications give rise to

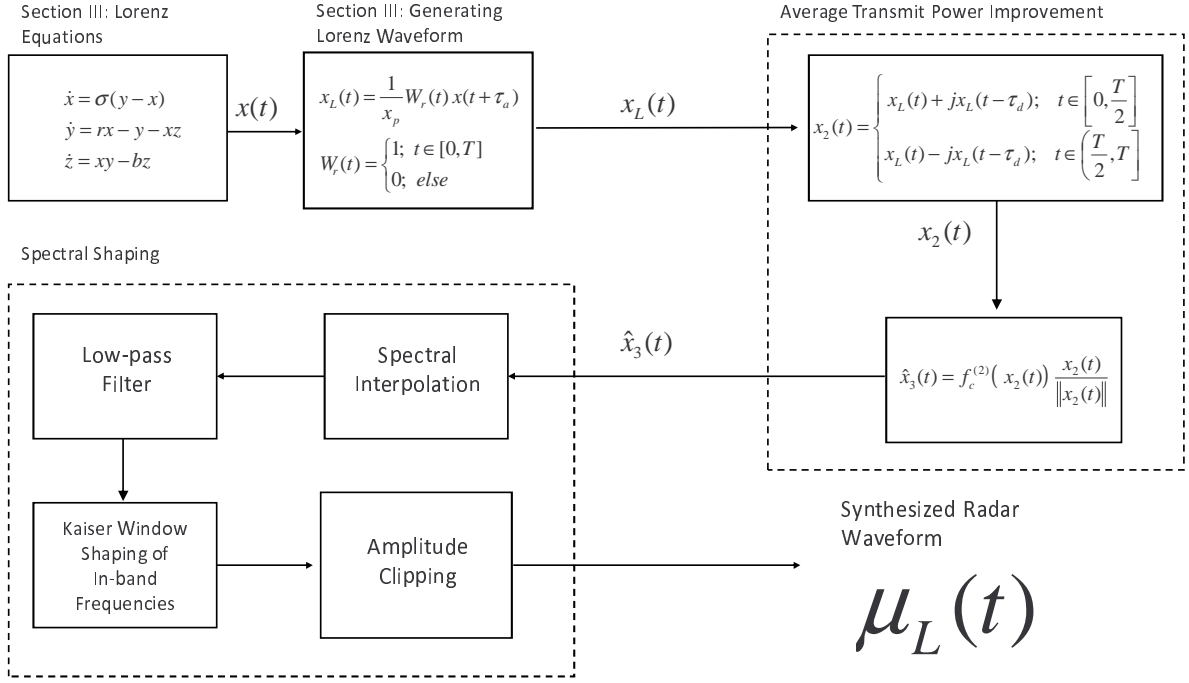


Fig. 7. Systematic Procedure for Generating Lorenz-Based Waveforms.

a procedure that provides Lorenz-based waveforms<sup>7</sup>, which perform equally, and in some cases better than, the pseudo-random noise waveforms presented in the previous section.

#### A. Average Transmit Power Improvement

Typically, the complex envelope includes both real and imaginary components so that the average power is close to the peak power (PRMS  $\approx 1$ ). Since the Lorenz waveform is a real-valued signal at baseband, adding an imaginary component can potentially increase the average power without significantly increasing the peak power of the waveform. For example, a real cosine signal has a PRMS of approximately 1.414. However, if a sine signal - which is a time-delayed replica of a cosine signal - is added as the imaginary component, the PRMS of the resulting complex exponential is 1. Similarly, as shown in Eq. 15, adding an imaginary component - equal to a time-delayed replica of the real component - to the original Lorenz waveform reduces the PRMS of the resulting waveform by aligning less energetic regions of one component with more energetic regions of the other. The parameter  $\tau_d$  in Eq.

<sup>7</sup>Other procedures for modifying Lorenz waveforms could certainly be formulated and, depending on the specifics of the radar system and application, these formulations could be more desirable than the one presented in this section.

15 can be determined empirically from the  $x$  state variable of the Lorenz system<sup>8</sup>.

$$x_1(t) = x_L(t) + jx_L(t - \tau_d) \quad (15)$$

Unfortunately, using a time-delayed replica of the real component as an imaginary component gives rise to high autocorrelation function sidelobes. However, slightly modifying the imaginary component of  $x_1(t)$  (according to Eq. 16) prevents the high autocorrelation function sidelobes while also achieving the same reduced PRMS as  $x_1(t)$ . The new complex signal,  $x_2(t)$ , is defined in Eqs. 16 and 17.

$$\tilde{x}(t) = \begin{cases} x_L(t - \tau_d); & t \in [0, \frac{T}{2}] \\ -x_L(t - \tau_d); & t \in (\frac{T}{2}, T] \\ 0; & \text{else} \end{cases} \quad (16)$$

$$x_2(t) = x_L(t) + j\tilde{x}(t) \quad (17)$$

To further reduce the PRMS, a mapping is introduced to amplify the low-power time segments of  $x_2(t)$ . Although many such mappings exist, the PRMS is adequately reduced using the mapping in Eq. 18 (where  $\|\cdot\|$  denotes  $\sqrt{(\cdot)(\cdot)^*}$ ).

$$f_c(x) = \sin \left( \frac{\pi \sqrt{\|x\|}}{2 \max [\sqrt{\|x\|}]} \right) \quad (18)$$

The mapping is applied as shown in Eq. 19 where  $f_c^{(2)}(\cdot) = f_c(f_c(\cdot))$ .

$$\hat{x}_3(t) = f_c^{(2)}(x_2(t)) \cdot \frac{x_2(t)}{\|x_2(t)\|} \quad (19)$$

Whereas the first term of Eq. 19 is used to map the amplitude of  $x_2(t)$  to the amplitude of  $\hat{x}_3(t)$ , the second term of Eq. 19 is required so that the phase for  $\hat{x}_3(t)$  is equal to the phase of  $x_2(t)$ .

When compared to the PRMS of the original Lorenz waveform, the PRMS of the resulting waveform,  $\hat{x}_3(t)$ , is significantly reduced. For a set of ten distinct waveforms, the average PRMS and maximum PRMS were 1.0140 and 1.0144, respectively. Now that the PRMS ratio is at an acceptable level, the spectrum of  $\hat{x}_3(t)$  can be shaped to decrease the autocorrelation function mainlobe width.

### B. Spectral Shaping

Properly shaping the spectrum of  $\hat{x}_3(t)$  by increasing its bandwidth will decrease autocorrelation function mainlobe width. Achieving the desired width is realized by shaping the in-band frequencies of the spectrum to approximately match a window function whose Fourier transform has a known mainlobe width. In this section, a Kaiser window is used and the Kaiser parameter  $\beta$  roughly controls the autocorrelation function width of the waveform. An advantage to using a Kaiser window is that it trades off mainlobe width with sidelobe area [21].

<sup>8</sup>Section 4.2 of [16] explains that the Lorenz waveform consists of consecutive peaks, which are separated by roughly the same time difference. This regular spacing allows alignment of peaks of the real signal with the nulls of the imaginary signal and vice versa.

To give the spectrum of  $\hat{x}_3(t)$  the shape of a Kaiser window, it is first expanded with spectral interpolation<sup>9</sup>. Expanding the spectrum is helpful in increasing the waveform's bandwidth but also increases the out-of-band energy. Consequently, after expanding the spectrum, the waveform is low-pass filtered to attenuate this out-of-band energy. Next, the in-band content of the energy spectrum is divided by the periodogram of the waveform, which normalizes the coarse trends of the energy spectrum. Next, a Kaiser window, with  $\beta = 4.75$ , is applied by multiplying the in-band frequencies of the spectrum with this window. This particular value of  $\beta$  was chosen so that the autocorrelation mainlobe width of the resulting waveform equaled that of the pseudo-random noise waveforms introduced in the previous section. Division by the periodogram and multiplication by the Kaiser window are implemented by applying a filter calculated with spectral factorization.

Since shaping the spectrum increases the PRMS of the output waveform, the amplitude of the shaped signal is clipped to reduce the PRMS back to an acceptable level<sup>10</sup>. The PRMS of the resulting waveform,  $\mu_L(t)$ , was calculated for 10 different waveforms and the mean PRMS and maximum PRMS were 1.22 and 1.26, respectively.

As shown in this section, the original Lorenz waveform,  $x_L(t)$ , can be modified in a systematic way to decrease both the PRMS and the mainlobe width of the autocorrelation function. The systematic procedure developed herein is shown in Fig. 7. The new, Lorenz-based waveform,  $\mu_L(t)$ , will be evaluated in the next section.

## VI. EVALUATING THE TRANSFORMED LORENZ RADAR WAVEFORMS

The modified Lorenz-based waveforms,  $\mu_L(t)$ , perform much better than the original Lorenz waveforms, and in some ways, outperform the pseudo-random noise waveform  $w(t)$ . Moreover, each waveform can be quickly generated - requiring only a few seconds when generated on a desktop machine running Matlab. While the computational complexity of this technique was not studied in great detail, efficient implementation in a radar system could allow waveforms to be generated on a pulse-to-pulse basis. A detailed evaluation of the modified Lorenz-based waveforms is given in this section.

### A. Average Transmit Power

As mentioned earlier the mean PRMS of  $\mu_L(t)$  over ten distinct waveforms is 1.22 and the peak value is 1.26. Since the PRMS of  $w(t)$  is 1.21, the PRMS of the modified Lorenz-based waveforms is roughly equal in value to that of  $w(t)$ . Thus, the average transmit power of both waveforms is within 5 dB of peak transmit power<sup>11</sup>.

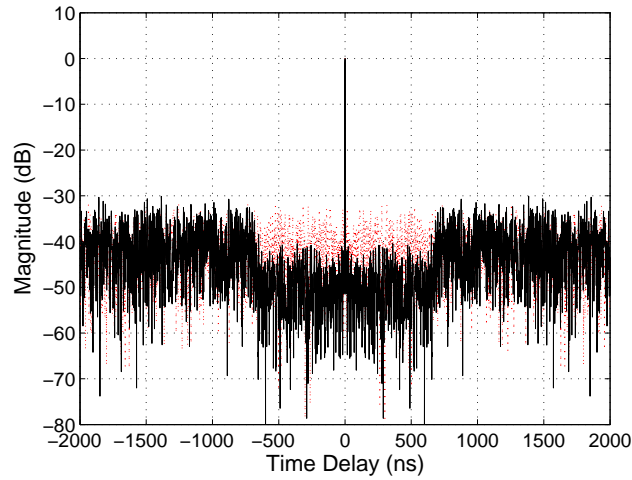
### B. Range Resolution and Sidelobes

As a result of the spectral shaping, the autocorrelation function of the modified Lorenz-based waveform demonstrates a mainlobe width approximately equal to that of  $w(t)$  and lower sidelobes than that of  $w(t)$  for a

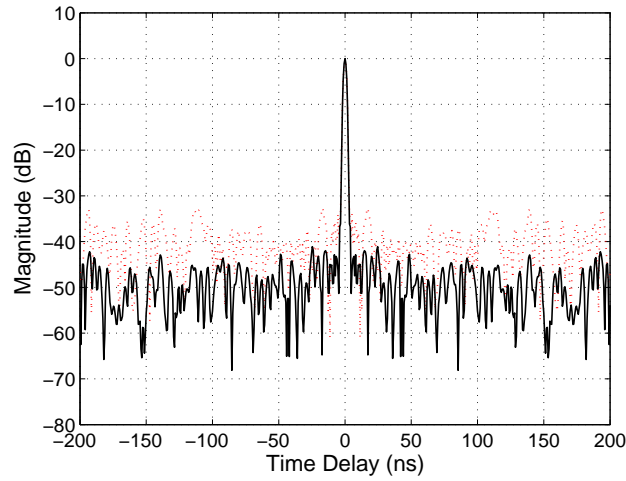
<sup>9</sup>Alternatively, the original waveform could be generated with a larger bandwidth.

<sup>10</sup>Although this amplitude clipping increases the out-of-band energy, plots in the next section illustrate that the resulting waveforms still possess an adequately compact spectrum.

<sup>11</sup>In the appendix of [16], the average transmit power of modified Lorenz-based waveform can be improved to about 3.56 dB less than peak transmit power by slightly modifying the generating procedure to produce real-valued waveforms.



(a)



(b)

Fig. 8. The Normalized Autocorrelation Function of  $\mu_L(t)$ . This figure plots the normalized autocorrelation function of  $\mu_L(t)$ ,  $r_{\mu_L\mu_L}(t)$ , with a solid line. The normalized autocorrelation function of  $w(t)$ ,  $r_{ww}(t)$  is plotted in the background with a dashed line. The second plot is an enlarged view of the first plot.

region surrounding the mainlobe. Outside this low sidelobe region, the level of the autocorrelation function sidelobes is roughly equal for both waveforms and is approximately equal to  $-10 \log(TB)$  dB. Plots of the autocorrelation function for both waveforms in Fig. 8 demonstrate both the narrow mainlobe and low sidelobes of  $\mu_L(t)$ . The autocorrelation function is plotted alongside the autocorrelation function of  $w(t)$  to demonstrate the lower sidelobes of the autocorrelation function of  $\mu_L(t)$ .

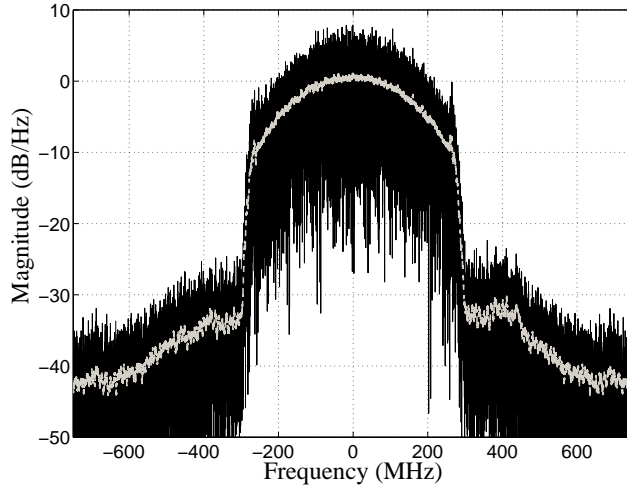


Fig. 9. The Normalized Energy Spectrum of  $\mu_L(t)$ . The black line is the energy spectrum of a typical transmit waveform and is calculated using Eq. 5. The gray line is used to approximate the average spectrum level for the set of waveforms and is calculated by smoothing the spectrum of a sample transmit waveform.

### C. Spectral Leakage

The triangular-like energy spectrum of the original Lorenz waveform (given in Fig. 3) has been modified to increase the waveform bandwidth. The energy spectrum for a typical modified Lorenz-based radar waveform is given in Fig. 9, which was computed via Eq. 5. This compact spectrum leads to a narrow autocorrelation function mainlobe width while still preventing significant spectral leakage.

### D. Orthogonality

As can be shown empirically, the Lorenz waveforms remain quasi-orthogonal since the cross-correlation level of the modified Lorenz-based radar waveform is unaffected by the operations that modify  $x_L(t)$ . The cross-correlation function of two distinct waveforms,  $\mu_{L1}(t)$  and  $\mu_{L2}(t)$ , is shown in Fig. 10 with the autocorrelation function of one of the waveforms in the background for comparison. The time-bandwidth product is  $10 \log_{10}(10^4) = 40\text{dB}$ , and the average cross-correlation level as expected, is calculated to be  $-44.56\text{ dB}$ . Thus, the modified Lorenz-based waveform comprise a quasi-orthogonal set.

## VII. CONCLUSIONS

As shown in this paper, a systematic waveform generating procedure based on the Lorenz system can be utilized to generate a set of quasi-orthogonal waveforms that can be systematically improved to yield output waveforms with the desired properties. Specifically, these waveforms possess normalized autocorrelation and cross-correlation function sidelobes are roughly equal to  $-10 \log(TB)\text{ dB}$  as well as a well-shaped energy spectrum that leads to a narrow autocorrelation mainlobe width and reduced spectral leakage. These waveforms also achieve an average transmit power within a few dB of peak power. Furthermore, since solutions to the Lorenz equations are uniquely

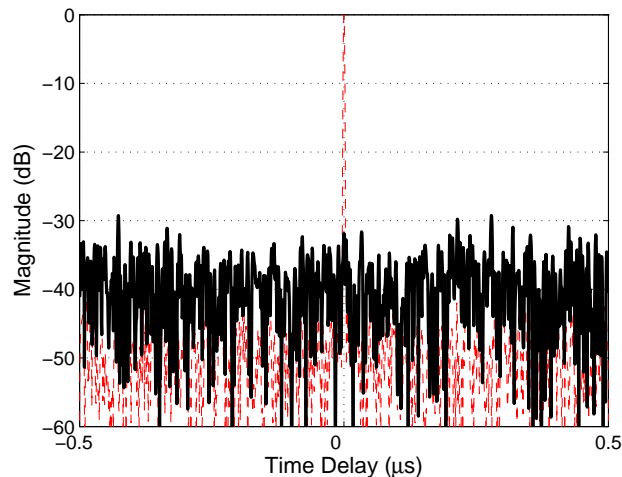


Fig. 10. Normalized Cross-Correlation Function of Two Distinct Lorenz-based Waveforms. The normalized cross-correlation function (solid line) is roughly equal to  $-10 \log(TB) = -40$  dB. The normalized autocorrelation function is plotted (dashed line) lightly in the background for reference.

specified by three Lorenz parameters and three initial conditions, each resulting waveform can be represented with just 6 parameters. This compressed representation and the limited computational complexity required to generate these waveforms could allow waveform generation on a pulse-by-pulse basis.

#### ACKNOWLEDGMENT

This work was sponsored in part under Air Force Contract FA8721-05-C-0002. Opinions, interpretations, recommendations and conclusions are those of the authors and are not necessarily endorsed by the United States Government. This work was supported in RLE in part by BAE Systems PO 112991, Lincoln Laboratory PO 7000032361, and the Texas Instruments Leadership University Program. The authors would like to thank the Siebel Foundation for the funding from the Siebel Scholarship Program. A special thanks goes to Dr. Frank Robey at M.I.T. Lincoln Laboratory for his help and support. Additionally, the contributions from all the members of the Digital Signal Processing Group at M.I.T. and Group 33 at M.I.T. Lincoln Laboratory were also appreciated.

#### REFERENCES

- [1] D. O. North, "An analysis of the factors which determine signal-noise discrimination in pulsed carrier systems," RCA Lab., Rep. PTR-6C; reprinted in *Proc. IEEE*, vol. 51, pp. 1016-1027, July 1963.
- [2] A. W. Rihaczek. *Principles of High-Resolution Radar*, volume 42 of *Applied Mathematical Sciences*. Artech House, Norwood, Massachusetts, 1996.
- [3] R. C. Dixon. *Spread Spectrum Systems*. John Wiley & Sons Inc., second edition, 1984.
- [4] P. M. Woodward. *Probability and Information Theory with Applications to Radar*, Pergamon, London, England, 1953.
- [5] M. I. Skolnik. *Radar Handbook*. McGraw-Hill, second edition, January 1990.
- [6] Frank C. Robey, Scott Coutts, Dennis Weikle, Jeffrey C. McHarg, and Kevin M. Cuomo. MIMO radar theory and experimental results. in *Signals, Systems and Computers*, 2004. Conference Record of the Thirty-Eighth Asilomar Conference, (Pacific Grove, CA), 2004.



- [7] G. San Antonio and D. R. Fuhrmann, "Beampattern synthesis for wideband MIMO radar systems," in *1st IEEE Int. Work. CAMSAP*, Puerto Vallarta, Mexico, Dec. 2005, pp. 105-108.
- [8] A. S. Luce, H. Molina, D. Muller, and V. Thirard, "Experimental results on RIAS digital beamforming radar," in *Proc. International Radar Conference*. Brighton, Eng: IEE, Oct 12-13 1992, pp. 74-77.
- [9] G. J. Frazer, Y. I. Abramovich, and B. A. Johnson, "Spatially Waveform Diverse Radar: Perspectives for High Frequency OTHR," in *Proc. Radar Conference*. Boston, MA, USA: IEEE, Apr 17-20 2007.
- [10] Y. I. Abramovich, G. J. Frazer, "Bounds on the Volume and Height Distributions for the MIMO Radar Ambiguity Function," *IEEE Signal Processing Letters*, vol. 15, pp. 505-508, 2008.
- [11] R. M. Narayanan, Y. Xu, P. D. Hoffmeyer, and J. O. Curtis. "Design, performance, and applications of a coherent ultra-wideband random noise radar," *Opt. Eng.*, pp. 1855-1869, 1998.
- [12] S. R. J. Axelsson. "Noise radar for range/Doppler processing and digital beamforming using low-bit ADC," *IEEE Trans. Geosci. Rem. Sens.*, vol. 41, pp. 2703-2720, 2003.
- [13] S. V. Marić and E. L. Titlebaum, "A class of frequency hop codes with nearly ideal characteristics for use in multiple-access spread-spectrum communications and radar and sonar systems," *IEEE trans. Communications*, vol. 40, pp. 1442-1447, 1992.
- [14] K. A. Lukin. "Millimeter wave noise radar applications: Theory and experiment," in *Proc. MSMW*, pp. 68-73, 2001.
- [15] B. C. Flores, E. A. Scolis, and G. Thomas. "Assessment of chaos-based FM signals for range-Doppler imaging," *IEE Proc. Radar Sonar Navig.*, vol. 150, pp. 313-322, 2003.
- [16] M. S. Willsey. Quasi-Orthogonal Wideband Radar Waveforms Based on Chaotic Systems. Master of Engineering thesis, Massachusetts Institute of Technology, 77 Massachusetts Avenue, Cambridge, MA 02139, December 2006.  
Available at: <http://www.rle.mit.edu/dspg/documents/mattnewthesis.pdf>
- [17] S. H. Strogatz. *Nonlinear Dynamics and Chaos*. Addison-Wesley, 1994.
- [18] K. M. Cuomo. Analysis and synthesis of self-synchronizing chaotic systems. Doctoral thesis, Massachusetts Institute of Technology, 77 Massachusetts Avenue, Cambridge, MA 02139, February 1994.
- [19] E. N. Lorenz. Deterministic nonperiodic flow. *Journal of the Atmospheric Sciences*, 20:130-141, March 1963.
- [20] William McC. Siebert. *Circuits, Signals, and Systems*. The MIT Electrical Engineering and Computer Science Series. The MIT Press, 1986.
- [21] A. V. Oppenheim and R. W. Schaffer. *Discrete-Time Signal Processing*. Signal Processing Series. Prentice Hall, Upper Saddle River, New Jersey, 1999.

**Matt S. Willsey** Matt S. Willsey attended the Massachusetts Institute of Technology where he received his B.S. degree in electrical science and engineering in 2005 and his M.Eng. degree in electrical engineering and computer science in 2007.

Mr. Willsey was a graduate student at the Research Laboratory of Electronics at M.I.T. during this project, and his research interests included waveform design, nonlinear dynamics, and MIMO radar systems. He is currently employed as an Engineering Scientist at the Applied Research Laboratories, the University of Texas at Austin (ARL:UT). At ARL:UT, his research is focused on signal processing applications for sonar systems. He was the recipient of the Siebel Scholarship in 2005 and is a member of Tau Beta Pi, Eta Kappa Nu, and Sigma Xi.

**Kevin M. Cuomo** Kevin M. Cuomo received the B.S. (magna cum laude) and M.S. degrees in electrical engineering from the State University of New York (SUNY) at Buffalo, in 1984 and 1986, respectively, and the Ph.D. degree in electrical engineering from Massachusetts Institute of Technology (MIT), Cambridge, in 1994.

He is a Senior Staff Member in the Ranges and Test Bed Group, MIT Lincoln Laboratory, where he works on the development of advanced signal processing methods for various radar applications. Before joining Lincoln Laboratory in 1988, he was a member of the research staff at Calspan Corporation, Buffalo, NY. He has authored several technical papers and reports in the areas of super resolution data processing and applications of chaotic dynamical systems for radar and communications. Recent research efforts include the development of super orthogonal waveforms for Multiple-Input Multiple-Output (MIMO) radar and corresponding beam space signal processing techniques.

Dr. Cuomo was awarded Departmental Honors and was the recipient of a University Fellowship and a Hughes Fellowship while attending SUNY Buffalo. He is a member of Tau Beta Pi, Eta Kappa Nu, and Sigma Xi.

**Alan V. Oppenheim** Alan V. Oppenheim was born in New York, New York on November 11, 1937. He received S.B. and S.M. degrees in 1961 and an Sc.D. degree in 1964, all in Electrical Engineering, from the Massachusetts Institute of Technology. He is also the recipient of an honorary doctorate from Tel Aviv University.

In 1964, Dr. Oppenheim joined the faculty at MIT, where he is currently Ford Professor of Engineering. Since 1967 he has been affiliated with MIT Lincoln Laboratory and since 1977 with the Woods Hole Oceanographic Institution. His research interests are in the general area of signal processing and its applications. He is coauthor of the widely used textbooks *Discrete-Time Signal Processing* and *Signals and Systems*. He is also editor of several advanced books on signal processing.

Dr. Oppenheim is a member of the National Academy of Engineering, a fellow of the IEEE, and a member of Sigma Xi and Eta Kappa Nu. He has been a Guggenheim Fellow and a Sackler Fellow. He has received a number of awards for outstanding research and teaching, including the IEEE Education Medal, the IEEE Jack S. Kilby Signal Processing Medal, the IEEE Centennial Award and the IEEE Third Millennium Medal. From the IEEE Signal Processing Society he has been honored with the Education Award, the Society Award, the Technical Achievement Award and the Senior Award. He has also received a number of awards at MIT for excellence in teaching, including the Bose Award and the Everett Moore Baker Award.